Don't Miss Weak Packets: Boosting LoRa Reception with Antenna Diversities

NINGNING HOU, XIANJIN XIA, and YUANQING ZHENG, The Hong Kong Polytechnic University, China

LoRa technology promises to connect billions of battery-powered devices over a long range for years. However, recent studies and industrial deployment find that LoRa suffers severe signal attenuation because of signal blockage in smart cities and long communication ranges in smart agriculture applications. As a result, weak LoRa packets cannot be correctly demodulated or even be detected in practice. To address this problem, this paper presents the design and implementation of MALoRa: a new LoRa reception scheme which aims to improve LoRa reception performance with antenna diversities. At a high level, MALoRa improves signal strength by reliably detecting and coherently combining weak signals received by multiple antennas of a gateway. MALoRa addresses a series of practical challenges, including reliable packet detection, symbol edge extraction, and phase-aligned constructive combining of weak signals. Moreover, MALoRa can also be applied to mobile devices. Experiment results show that MALoRa can effectively expand communication range, increase battery life of LoRa devices, and improve packet detection and demodulation performance especially in ultra-low SNR scenarios.

CCS Concepts: • **Networks** → **Network protocol design;**

Additional Key Words and Phrases: IoT, LPWAN, LoRa, weak packet detection, multiple antenna

ACM Reference format:
Ningning Hou, Xianjin Xia, and Yuanqing Zheng. 2023. Don't Miss Weak Packets: Boosting LoRa Reception with Antenna Diversities. *ACM Trans. Sen. Netw.* 19, 2, Article 41 (February 2023), 25 pages.
https://doi.org/10.1145/3563698

1 INTRODUCTION

Low-Power Wide-Area Networks (LPWANs) such as LoRaWANs are promising technologies to connect billions of devices and enable large scale applications (e.g., waste management, wildlife tracking, shipping and transportation scheduling, disaster rescue, etc.) [1–8]. LoRa adopts **chirp spread spectrum (CSS)** modulation in **physical layer (PHY)**, which is resilient and robust to interference and noise. LoRa is expected to achieve up to 10 km communication range with battery-powered devices working for years. However, recent studies [9–13] find that the communication range of LoRa falls short of industry needs and expectations in real-world application scenarios.

This work is supported in part by Hong Kong General Research Fund (GRF) under grant PolyU 152165/19E and 15218022, in part by the Start-up Fund for Research Assistant Professor (RAP) under the Strategic Hiring Scheme of Hong Kong PolyU under grant P0036217, and in part by the National Nature Science Foundation of China (NSFC) under Grant No. 62102336.
Authors' address: N. Hou, X. Xia, and Y. Zheng (corresponding author), 11 Yuk Choi Road, Hung Hom, KLN, Hong Kong; emails: ningning.hou@connect.polyu.hk, {xianjin.xia, yqzheng}@polyu.edu.hk.

1550-4859/2023/02-ART41 $15.00
https://doi.org/10.1145/3563698

Table 1. Comparison between MALoRa and Recent Studies

	Storage Overhead	Running Time	Communication Overhead	Symbol-level Synchronization	SNR Gain	SER	Multi-Antenna
Charm [11]	large	5.07 ms	high	high	1–3 dB	0.50	No
NELoRa [15]	large	7.19 ms	low	low	1.8–2.4 dB	0.91	No
MALoRa	small	0.63 ms	low	high	1.3–6.6 dB	0.03	Yes

For example, LoRa devices deployed in urban environments or remote areas suffer severe signal attenuation due to signal blockage and long propagation distance. As a result, the **Signal-to-Noise ratio (SNR)** of LoRa packets can be severely degraded, leading to decoding failures at gateways and rapid battery drain of LoRa nodes. Suffering from low SNRs, weak packets of devices located deep inside buildings [14] may not even be detected, let alone decoded at nearby gateways separated by a number of concrete walls.

Current LoRaWAN adapts data rates in hopes of crossing an SNR threshold at minimum power consumption. However, some devices can still be out of reach even with the most conservative parameter settings. In this paper, we aim to improve the LoRa packet reception performance in ultra-low SNR scenarios without extra power consumption of battery-powered LoRa transmitters.

Latest studies Charm [11] and NELoRa [15] also work on low-SNR packet reception. Charm proposes to aggregate weak physical layer samples from multiple distributed gateways. This approach incurs high network traffic and high computation overhead since a large volume of raw samples need to be uploaded to a centralized server. Besides, Charm requires sample-level synchronization among distributed gateways, which is extremely hard to achieve in practice. NELoRa proposes a neural-enhanced demodulation method that makes use of a deep learning framework to decode received LoRa PHY samples. NELoRa needs to be pre-trained with high sampling rate data, which is computationally intensive. NELoRa also requires different deep learning models to demodulate packets with different parameter settings. The storage and computation overhead become larger as SF is getting larger. In specific, we use the same settings as used in NELoRa and measure the time of processing 16 chirp symbols on a PC platform when $SF = 7$ and $BW = 125$ kHz. As summarized in Table 1, Charm and NELoRa suffer from large storage overhead and computation overhead, and the overall SERs in low-SNR conditions are high.

As illustrated in Figure 1, we propose to leverage multiple antennas of a gateway to coherently combine the received signals from a LoRa transmitter so as to improve the packet reception performance. Although simple in concept, it entails tremendous technical challenges in the design and implementation of such a multi-antenna LoRa gateway. First, under ultra-low SNR scenarios, the received signals at each antenna can be very weak and submerged below the noise floor. In this case, the weak packets may not be detected. Second, in order to achieve coherent combining, the received signals should be aligned and constructively combined. Traditional channel sounding methods cannot be applied in the ultra-low SNR scenarios, since noise level could be too high for accurate channel measurement. Besides, the channel measurement could incur extra power consumption which cannot be afforded by battery-powered transmitters.

Current LoRa gateways detect the arrival of LoRa packets by detecting LoRa preambles, which consist of a few up-chirps. The preamble detection methods correlate an up-chirp with incoming signals and count the number of repetitive correlation peaks. A LoRa packet can thus be detected if multiple correlation peaks can be observed periodically. However, such methods do not work well in ultra-low SNR scenarios, since weak correlation peaks can be submerged below noise floors.

To improve the weak packet detection performance, we propose to fully leverage multiple up-chirps in LoRa preambles. While the energy of one chirp may be overwhelmed by noise, the energy

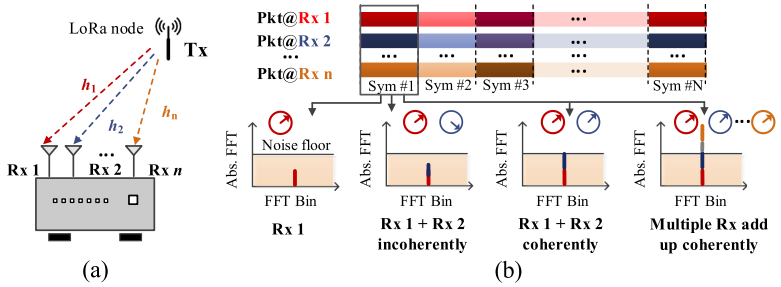

Fig. 1. Illustration of the high level idea of MALoRa. (a) Multiple Rx antennas provide multiple phase-shifted signals of a packet, (b) Coherent combining of multiple antennas helps a gateway constructively add up the signals and improve SNR.

of multiple chirps can be aggregated to improve the packet detection performance. Intuitively, we can combine multiple consecutive up-chirps by increasing the packet detection window size in a way that the energy of multiple up-chirps can add up constructively. However, if all up-chirps are aggregated into one detection window, we cannot observe a certain number of periodic peaks anymore, which could lead to more false alarms. Fortunately, LoRa standard allows us to dynamically adapt and configure the preamble length of a LoRa packet before transmission. We configure the number of up-chirps in a LoRa preamble and the packet detection window to strike a balance between packet detection sensitivity and robustness.

Coherent combining has been extensively studied in wireless systems (e.g., WiFi [16, 17], 5G [18]). Such works typically measure the wireless channels between a transmitter to multiple antennas, which involves high communication and computation overhead and require relatively good channel conditions to achieve accurate channel measurements. Besides, to reduce the power consumption of LoRa transmitters, the inter-packet interval of LoRa transmitters are much longer than those of other wireless systems (e.g., WiFi, 5G), which make the channel measurement become easily obsolete and cannot be used for coherent combining.

To enable coherent combining of weak LoRa signals, we propose a novel phase difference measurement method that allows us to well-align phase-shifted copies of LoRa signals received at multiple antennas of a gateway. Unlike existing wireless channel measurement methods, we aim to accurately measure the phase differences between multiple wireless channels under ultra-low SNRs. To this end, we leverage the unique feature of LoRa to improve the phase difference measurement performance. Since LoRa preamble chirps share the same wireless channel as the payload chirps, we can exploit consecutive preamble chirps to accurately measure the phase shifts between wireless channels and compensate for payload chirps in coherent combining. As illustrated in Figure 1, once the phase differences can be accurately measured, we can coherently combine the phase-shifted copies of weak LoRa signals in a way that the SNR-enhanced LoRa signals can eventually cross the SNR threshold for successful packet reception. Besides, we present an enhanced method for channel measurement in mobility scenarios, which can improve the stability of MALoRa and expand the application of MALoRa to both static and mobile devices.

We prototype MALoRa as a software-defined gateway with multiple synchronized USRPs. We evaluate MALoRa with commodity LoRa nodes in both indoor and outdoor environments. We comprehensively evaluate the performance of MALoRa in packet detection, symbol demodulation, SNR gain, and energy saving. Experiment results show that MALoRa can substantially improve packet detection and demodulation performance, and outperform the state-of-the-art benchmarks especially under ultra-low SNRs.

We summarize the key contributions as follows:

- We propose a novel technique that leverages the unique features of LoRa chirps and LoRa packet structure to improve the packet detection performance in ultra-low SNR environments.
- We propose a new phase difference measurement method that can be used to accurately measure phase differences between multiple wireless channels and coherently combine weak LoRa signals received by multiple antennas of a gateway.
- We design and implement a prototype of MALoRa with software-defined radios and conduct comprehensive evaluations in various experiment settings. The experiment results with commodity LoRa nodes demonstrate that MALoRa can substantially improve weak packet reception performance especially under ultra-low SNR scenarios.

2 LORA PRIMER

Chirp Spread Spectrum (CSS). LoRa adopts Chirp Spread Spectrum (CSS) modulation in physical layer. In CSS, a chirp signal sweeps through a bandwidth with an instant frequency increasing (up-chirp) or decreasing (down-chirp) linearly at a constant rate $k = \frac{BW^2}{2^{SF}}$, where SF represents the spreading factor. A *base chirp* sweeps from $-\frac{BW}{2}$ to $\frac{BW}{2}$ and can be represented as $C(t) = e^{j2\pi(\frac{k}{2}t-\frac{BW}{2})t}$. LoRa changes the initial frequency to modulate data with different symbols as follows

$$S(t, f_{sym}) = C(t) \cdot e^{j(2\pi f_{sym}t+\varphi_{sym})}, \tag{1}$$

where f_{sym} and φ_{sym} denote the initial frequency and initial phase of the chirp signal, respectively.

LoRa demodulation. A LoRa receiver demodulates a symbol by extracting the initial frequency of a LoRa chirp. We represent a received symbol with noise as below.

$$y(t) = h \cdot S(t, f_{sym}) + n(t), \tag{2}$$

where h denotes the wireless channel between a transmitter and a receiver and $n(t)$ represents noises. To demodulate a symbol, LoRa first *de-chirps* the received signal by multiplying with the *conjugate of base chirp* denoted as $C^{-1}(t)$ and then performs **Fast Fourier Transform (FFT)** to extract f_{sym}. This process can be represented as $Z(f) = FFT(y(t) \cdot C^{-1}(t))$. The FFT peak in $Z(f)$ indicates f_{sym} and its corresponding symbol.

LoRa packet structure. As illustrated in Figure 2, a LoRa packet starts with a preamble which is composed of a varied number of base chirps, followed by two up-chirps as sync words, 2.25 down-chirps as a **start frame delimiter (SFD)** and the payload of the packet.

A LoRa receiver continuously monitors a channel to detect incoming packets. A receiver detects a LoRa packet by detecting the presence of LoRa preamble. When a preamble is detected, it further detects SFD and extracts frame timing information from preamble and SFD chirps to demodulate symbols in the payload of the packet.

3 MOTIVATION

Target application scenario. LoRa is promising to connect low-power IoT devices in a wide area thanks to its large link budget and high sensitivity of LoRa receiver radios. Commodity radio manufacturers advertise that LoRa radios can decode a packet over a long communication range even when the signal strength falls below noise floors [19]. However, recent studies [11, 20] find that the communication range of LoRa can be much shorter in urban environments due to dramatic power losses because of signal blockage and signal attenuation over long communication ranges. In this case, a commodity receiver can barely receive any packets from a LoRa node. This problem prohibits the wide adoption of LoRa technology in smart city applications, where reliable data

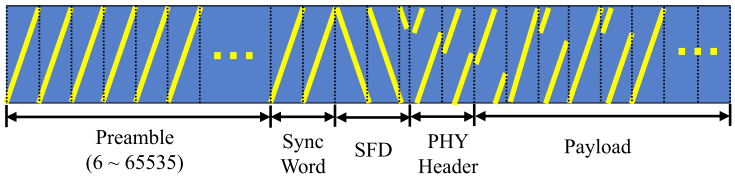

Fig. 2. LoRa packet structure. The preamble length is variable.

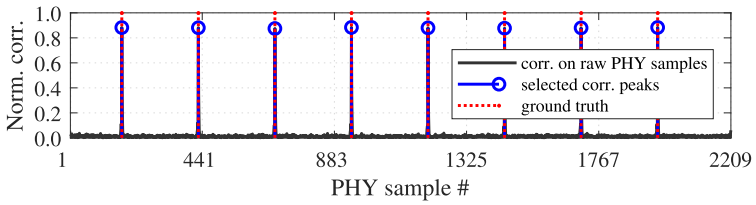

(a) Correlation results with high SNR

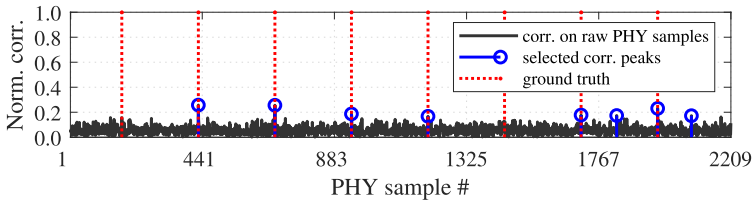

(b) Correlation results with low SNR

Fig. 3. Preamble correlation results for LoRa packet detection: (a) SNR = 0 dB; (b) SNR = −25 dB.

collection is essential yet challenging. Our work aims to fill this gap by supporting LoRa communications in such challenging environments with ultra-low SNRs. We believe improving the weak packet reception performance is critical to many real-world usage scenarios such as wild fire detection in remote field and intrusion detection in smart building which need infrequent but reliable data transfer – where weak packets should not be missed.

Problem with low-SNR LoRa reception. A LoRa radio requires a minimum SNR to correctly detect and receive a packet. If the SNR of a packet falls below the minimum requirement, the packet cannot be received. In the following, we empirically study the LoRa packet reception process and elaborate why it is challenging to receive a LoRa packet when SNR is low.

LoRa packet reception generally involves two key phases: (1) packet detection and (2) payload demodulation. Commodity LoRa radios detect packets with **Channel Activity Detection (CAD)** operation which detects LoRa preamble by correlating incoming signals with standard base chirps. Figure 3(a) and (b) compare preamble detection results in high and low SNRs. When SNR is high as presented in Figure 3(a), we observe periodic correlation peaks. A receiver can thus count the number of correlation peaks and detect incoming packets. However, when SNR decreases as shown in Figure 3(b), the correlation peaks drop dramatically and mess up with noise peaks. If SNR further decreases, current packet detection method may not even be able to detect any correlation peaks and separate them from noises. As such, conventional packet detection method fails in low SNR scenarios. If a packet cannot be detected due to low SNR in the packet detection phase, the LoRa receiver will skip the payload demodulation phase as if there were no incoming packet.

If a packet with sufficient SNR can be successfully detected, its payload chirps will be captured for symbol demodulation. Figure 4 examines the impacts of SNRs on symbol demodulation.

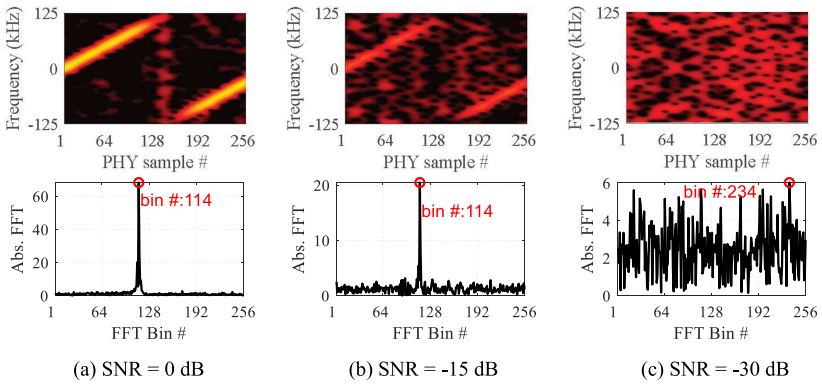

Fig. 4. Spectrogram and de-chirp FFT results of one chirp under different SNRs. The energy peak of a chirp is submerged by noise under ultra-low SNR.

Normally, we can correctly demodulate a symbol from the FFT results if SNR is sufficiently high. As shown in Figure 4(a), when SNR is 0 dB (a typical LoRaWAN scenario in short range), the conventional symbol demodulation method (i.e., multiplying with a down chirp and performing FFT) can detect the FFT peak and accomplish the demodulation task. Even when the SNR decreases below the noise floor such as −15 dB (a long range or wall penetrating scenario), the conventional demodulation method can sometimes work since the power of a LoRa chirp can be concentrated into a single FFT bin by multiplying with a down chirp as shown in Figure 4(b). As a result, we can still correctly demodulate the received symbol whose the initial frequency correspond to bin # 114 in the experiments. However, when SNR further decreases to −30 dB (ultra-low SNR scenario because of blockage of line-of-sight path or signal attenuation over a longer range), the conventional demodulation method cannot find the correct FFT peak any more, which leads to symbol errors in the demodulation phase.

Note that coding schemes (e.g., Hamming code, Gray code) are adopted in LoRa physical layer which are capable of correcting a small number of symbol errors (e.g., due to carrier frequency offsets). Such coding schemes however cannot save weak packets in such ultra-low SNR scenarios, since all payload chirps suffer high noises and excessive symbol errors. Similarly, retransmission could not help either, since the channel conditions would remain poor in ultra-low SNR scenarios. As a result, weak packets with low SNRs are more likely to be missed in both packet detection and payload demodulation phases.

Opportunity. Latest commodity gateways are equipped with multiple antennas [21–24]. In downlink transmissions (i.e., from a gateway to LoRa nodes), multiple antennas are used to transmit different messages to different LoRa nodes [25]. To support concurrent downlink transmission, antennas can be configured with orthogonal parameters (e.g., different channels [25]). As such, the downlink transmissions can happen without any collisions to LoRa nodes. In uplink reception, the multiple antennas work independently in packet detection and demodulation.

In this paper, we aim to fully leverage the multiple antennas of a gateway to improve the LoRa packet reception performance in ultra-low SNR scenarios. Intuitively, we propose novel techniques to add up the weak signals of multiple antennas and strengthen LoRa signals. Even if the signal SNRs may fall below SNR threshold of an individual antenna, we can still combine signals of multiple antennas to pull up SNRs above the threshold for correct packet demodulation. The more antennas we use, the higher SNR gains we may achieve.

4 DESIGN DETAILS

4.1 Packet Detection with Chirp Combination

The standard correlation based method (e.g., CAD of a LoRa radio) fails to detect weak packets in ultra-low SNRs as shown in Figure 3(b). In this subsection, we present a new method for weak LoRa packet detection in ultra-low SNRs.

We exploit the fact that a LoRa preamble consists of consecutive identical base chirps, which means that the dechirped signals of any preamble chirps would have the same frequency. When we perform FFT on the dechirped signals of a preamble chirp, the FFT result can be represented as below.

$$Z(m) = FFT(y(n) \cdot C^{-1}(n)) = \sum_{n=0}^{N_0-1} e^{-j2\pi \frac{mn}{N_0}} (x[n] + \hat{w}[n]), \tag{3}$$

where $Z(m)$ is the corresponding frequency component at bin m, N_0 is the length of discrete samples within a preamble up-chirp, and n indicates the n th discrete sample. We use $x[n] = hS[n]C^{-1}[n]$ to indicate the dechirped signals of symbol $S(t, f_{sym})$ and use $\hat{w}[n]$ to represent noises.

After FFT, the energy of a preamble chirp accumulates into a specific bin (e.g., m_0) corresponding to the frequency of the dechirped component. The magnitude of the frequency component $|Z_c(m_0)|$ can be calculated as below.

$$|Z_c(m_0)| = \left| \sum_{n=0}^{N_0-1} e^{-j2\pi \frac{m_0 n}{N_0}} x[n] \right| = hN_0 \tag{4}$$

We can observe from Equation (4) that the magnitude of the frequency component $|Z_c(m_0)|$ is proportional to the length of discrete samples within a dechirp window. As all preamble chirps produce the same frequency component after dechirping, if more samples from a longer signal duration (e.g., N preamble chirps) are put into an FFT, a higher FFT peak can be expected because the energy of samples from N chirps add up in one FFT bin. We can formally represent the procedure of using N chirps for preamble detection as follows.

$$|Z_c(m_N)| = \left| \sum_{n=0}^{N_0 N-1} e^{-j2\pi \frac{m_0 n}{N_0 N}} x[n] \right| = hN_0 N \tag{5}$$

Equation (5) depicts the FFT magnitude of an enlarged detection window with N preamble chirps. Comparing Equations (4) and (5), we can see an $N\times$ increase of the FFT peak. Due to an increased FFT resolution, the location of the FFT peak would change from m_0 to m_N, where $m_N = Nm_0$.

We now consider the noise component $\hat{w}[n]$. In general, it follows a compound Gaussian distribution [15, 26], where the image part $\Im(\hat{w}) \sim \mathcal{N}(0, \sigma^2)$ and the real part $\Re(\hat{w}) \sim \mathcal{N}(0, \sigma^2)$. The total energy of noise in a detection window of one chirp can be expressed as below.

$$E_w = \sum_{n=0}^{N_0-1} |\hat{w}[n]|^2 = N_0 \times E(|\hat{w}[n]|^2) = 2\sigma^2 N_0, \tag{6}$$

where $2\sigma^2$ is the expectation of the instant noise energy density. Equation (6) calculates the noise energy in time domain while Equation (7) represents it in frequency domain.

$$E_w = \frac{1}{N_0} \sum_{m=0}^{N_0-1} |Z_w(m)|^2 \tag{7}$$

$Z_w(m)$ is the **power spectral density (PSD)** of noises at a frequency bin m. According to Parseval's theorem, the total energy of signals in frequency domain should be equal to that in time

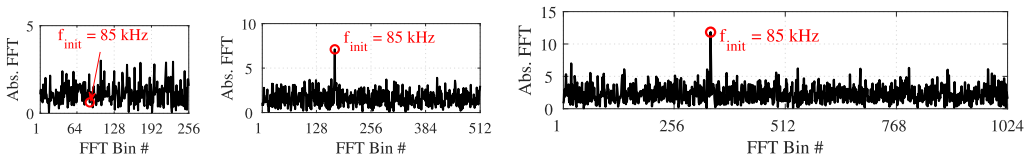

(a) Detection win = 1 chirp (b) Detection win = 2 chirps (c) Detection win = 4 chirps

Fig. 5. Packet detection with different lengths of detection windows: the larger the detection window, the higher the energy peak of the targeted chirp signal. We can increase detection window length to detect a packet in ultra-low SNR scenarios.

domain (i.e., Equation (6) = Equation (7)). As the PSD of Gaussian noise is subject to a uniform distribution, the average amplitude of noise peak at each FFT bin can be represented as

$$\overline{|Z_w(m_0)|} = \sqrt[2]{2\sigma^2 N_0}. \tag{8}$$

According to Equation (8), if we enlarge the detection window from one preamble chirp to N preamble chirps (i.e., increase discrete samples from N_0 to N_0N), the average noise level will increase by $\sqrt[2]{N}\times$. Consequently, the amplitude increase of the targeted chirp signal is much higher than that of noise. The rationale behind this is that the dechirp and FFT operations concentrate the energy of the targeted chirp signal in one single FFT bin but spread the noise energy throughout the whole spectrum. This motivates us to increase the length of detection window from one chirp to N chirps to detect a weak LoRa preamble.

Figure 5 shows the FFT results of dechirped signals of a weak preamble with different detection window sizes. We observe that though the energy of a single preamble chirp is submerged below noise floor as shown in Figure 5(a), the FFT peak of the dechirped preamble signals becomes higher as the detection window size increases from one chirp to four chirps as shown in Figure 5(b). As more preamble signals are used for FFT analysis, more signal energy accumulates and the resulting FFT peak grows higher. In contrast, the noise floor remains at almost the same level during the process because noise power will not accumulate in anyone of the FFT bins due to the randomness of noises. As a result, the energy of preamble signals (i.e., FFT magnitude) would gradually increase to surpass noise floor as more chirps are added into a detection window, as shown in Figure 5(b, c).

In practice, we use a sufficiently long detection window that accumulates the signal energy of N chirps to detect a weak LoRa preamble. To avoid false alarms, we slide a detection window across received signals. If the FFT peaks can be periodically detected multiple times in the same FFT bin when we slide the detection window to different offsets, we can then assure that a real LoRa preamble is present. To achieve real-time packet detection, MALoRa slides the detection window with a large offset per step. We empirically configure the sliding offset as one chirp duration per step in our implementation. It can effectively reduce computation overhead without missing most packets.

Figure 6 presents the detection results of a weak LoRa preamble (SNR=−25 dB) using a detection window in length of 4 chirps (i.e., $N = 4$). As we slide the detection window across the signals of the preamble, periodic high energy peaks are detected in the same frequency bin (e.g., $f = 0$) across different offset positions as shown in Figure 6(a). We plot the magnitude of the detected frequency (i.e., $f = 0$) in Figure 6(b). We see that the gap between detected peaks equals to the length of a chirp duration. The noise in between is very small. This periodic appearance of frequency peaks indicates the presence of a LoRa preamble. Note that the 5^{th} and 6^{th} peaks have lower amplitude compared with the first four peaks since these two peaks include the sync word(s) whose initial frequencies differ from that of preamble chirps. Here, the number of preamble chirps is 8.

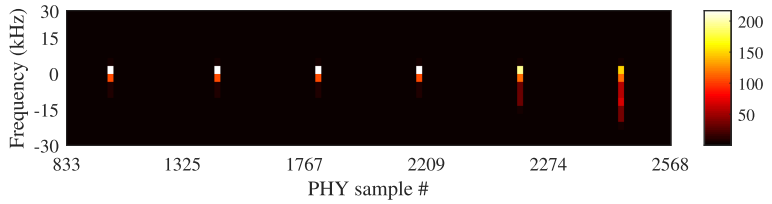

(a) Preamble detection with sliding windows

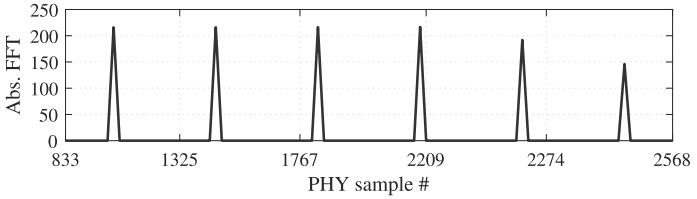

(b) Signal magnitude of freq. 0 across multiple detection windows

Fig. 6. Packet detection with a detection window in length of 4 chirps.

4.2 Packet Demodulation with Multiple Antennas

Though we can combine multiple preamble chirps to detect a weak LoRa packet, the same method cannot be used to decode the packet because chirps in the payload usually differ from each other. Instead, MALoRa coherently combines the signals of multiple antennas and leverages the SNR gains to demodulate and decode a weak packet. In the following, we first present how to measure channel difference between a transmitter to multiple antennas.

Measuring channel difference. Intuitively, we may extract channel h from a received LoRa symbol $y(t)$ according to Equation (2). We can first dechirp $y(t)$ and then extract the phase of channel from the FFT response of the demodulated symbol.

However, the raw phase measurement may contain not only channel phase, but also phase distortions incurred by radio hardware such as **Carrier Frequency Offset (CFO)** and **Sampling Timing Offset (STO)**. We cannot use existing methods to estimate and calibrate for those phase distortions because it is not likely to estimate the correct CFO and STO in ultra-low SNRs. Without loss of generality, we take the phase distortions of radio hardware into account and update the received signals of a LoRa symbol (i.e., Equation (2)) as below.

$$y(t) = h \cdot e^{j\varphi_{distort}(t)} \cdot S(t, f_{sym}) + n(t), \tag{9}$$

where $\varphi_{distort}(t)$ characterizes the phase distortions of radios including CFO, STO and phase jitters caused by hardware imperfection [4].

MALoRa uses two synchronized Rx antennas of a gateway to calibrate phase distortions in received low-SNR signals. Let $y_1(t)$ and $y_2(t)$ denote the signal copies received by two antennas. As the two antennas are synchronized in time, frequency and phase, $y_1(t)$ and $y_2(t)$ would have the same CFO, STO as well as the resulting phase distortions $\varphi_{distort}(t)$. Then, we can remove $\varphi_{distort}(t)$ by multiplying $y_1(t)$ with the conjugate of $y_2(t)$ denoted as $y_2^*(t)$, which is represented as follows.

$$y_1(t) \cdot y_2^*(t) = h_1 \cdot h_2^* + \widetilde{n}(t), \tag{10}$$

where $\widetilde{n}(t)$ denotes noises after conjugate multiplication. The phase of $h_1 \cdot h_2^*$ corresponds to the phase difference between channels h_1 and h_2, i.e., $\Phi(h_1 \cdot h_2^*) = \Phi(h_1) - \Phi(h_2)$, where $\Phi(\cdot)$ extracts the phase of a complex number.

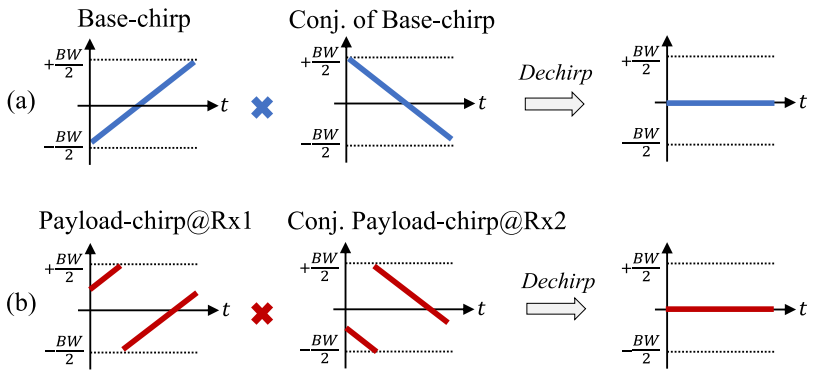

Fig. 7. Conjugate multiplication removes differences in base-band chirp signals. (a) Dechirp a standard preamble chirp, (b) Dechirp a payload-chirp with Rx pairs by multiplying the chirp received by Rx1 with the conjugate of the signal copy received by Rx2.

Ideally, we can use Equation (10) to directly measure the phase difference between $y_1(t)$ and $y_2(t)$ for coherent combining. However, in the case of ultra-low SNRs, the power strength of noises can be comparable with or even higher than the power of signals. As a result, $h_1 \cdot h_2^*$ may be submerged below noise floor and the phase measurement of $h_1 \cdot h_2^*$ would be distorted by $\widetilde{n}(t)$ in practice.

MALoRa pulls up SNRs of signal component $h_1 \cdot h_2^*$ by leveraging multiple chirps in LoRa preamble. Basically, as chirps in preamble are identical, we can use Equation (10) to extract the same $h_1 \cdot h_2^*$ from any preamble chirps of the two antennas. Although the signal energy of $h_1 \cdot h_2^*$ from a single chirp is submerged below the noise floor as shown in Figure 8(b), we can aggregate the signals (i.e., $h_1 \cdot h_2^*$) extracted from multiple preamble chirps to accumulate signal energy in one FFT bin. Figure 8(c) shows the FFT results when eight preamble chirps are added up constructively, where the peak at bin #1 corresponds to $h_1 \cdot h_2^*$. Comparing Figures 8(b) and 8(c), we see that the FFT peak of component $h_1 \cdot h_2^*$ emerges above the noise floor as the signal energy of $h_1 \cdot h_2^*$ from all preamble chirps accumulates in bin #1. Then we can accurately measure the phase of the emerging FFT peak representing $h_1 \cdot h_2^*$.

Since LoRa chirps of the same packet pass through the same wireless channel, we find that the same channel component ($h_1 \cdot h_2^*$) can also be obtained from other parts of a packet (e.g., sync words, SFD, and payload) in addition to preamble. Although chirps in other parts usually differ from each other and the preamble chirps (e.g., initial frequency), the difference of chirps can be removed by Equation (10). Since $y_1(t)$ and $y_2(t)$ in Equation (10) correspond to the same symbol received by two antennas, they share the same base-band chirp signal (i.e., $S(t, f_{sym})$). This chirp signal is removed during the process of conjugate multiplication (i.e., $y_1(t) \cdot y_2^*(t)$). As illustrated in Figure 7, the conjugate multiplication would produce the same results for both a preamble chirp and a payload symbol. The results produced by Equation (10) (i.e., $h_1 \cdot h_2^*$) are indeed chirp independent. The same channel component ($h_1 \cdot h_2^*$) can be extracted from different parts of the same packet (e.g., preamble and payload). As such, the signal components ($h_1 \cdot h_2^*$) extracted from different parts of the packet can be added up constructively to strengthen the signal energy of $h_1 \cdot h_2^*$. If chirps from both preamble and payload of a packet are aggregated to enhance SNRs for signal ($h_1 \cdot h_2^*$), we can expect to have sufficiently high signal energy to accurately measure the channel difference of two antennas.

Figure 8 presents the results of channel difference measurement from signals of a LoRa packet (SNR = -25 dB) received by two antennas. We see from Figure 8(a) that the signals (i.e., $h_1 \cdot h_2^*$) extracted from preamble, SFD and payload form a long horizontal line, indicating that the extracted signals have the same frequency (i.e., $f = 0$). As shown in Figure 8(b), the signal strength of ($h_1 \cdot h_2^*$)

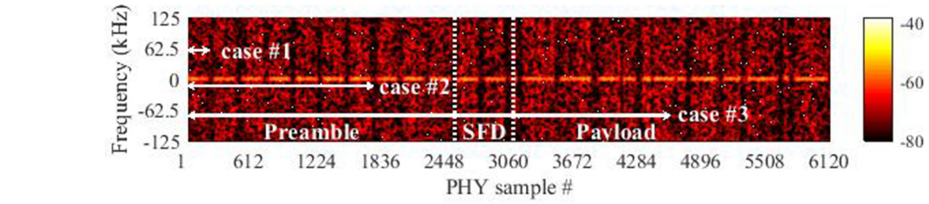

(a) Spectrum of the conjugate multiplication results of two Rx antennas

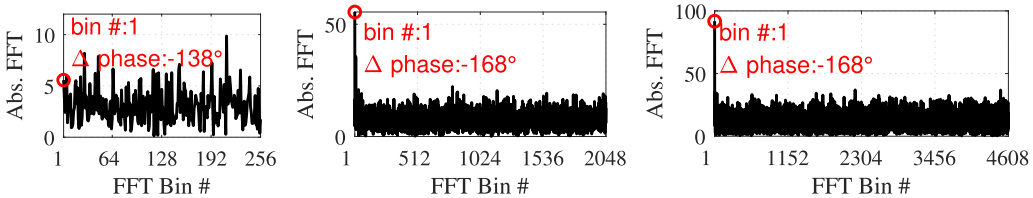

(b) Case #1 (c) Case #2 (d) Case #3

Fig. 8. Measuring channel difference with two synchronized antennas. (a) Spectrum of the conjugate multiplication results of an Rx pair: the energy of all chirps concentrates at zero frequency; (b-d) measuring channel difference with 1 preamble chirp (Case #1), 8 preamble chirps (Case #2), and 16 different kinds of chirps including preamble, SFD and payload chirps (Case #3), respectively.

extracted from a single chirp is below the noise floor, from which we cannot correctly measure the channel difference of the two antennas. When eight preamble chirps are aggregated together, the accumulated signal energy of $h_1 \cdot h_2^*$ increases above the noise floor as shown in Figure 8(c). Finally, when more chirps from both preamble and payload are aggregated, the FFT peak of $h_1 \cdot h_2^*$ grows higher as shown in Figure 8(d), from which the phase difference between channels h_1 and h_2 can be measured more reliably.

Coherent combining. After measuring the channel difference between any two antennas, we next combine multiple antennas to obtain SNR-enhanced signals.

Let $y_i(t)$ denote the received signals of the i^{th} antenna and $\Delta\phi_{ij}$ denote the phase difference between signals of the i^{th} and the j^{th} antennas. MALoRa compensates phase differences among signals of different antennas for coherent combining. The signal combination of M antennas is represented as below.

$$Y_{combine}(t) = y_1(t) + \sum_{i=2}^{M} y_i(t) \cdot e^{-j\Delta\phi_{i1}}, \tag{11}$$

where $y_i(t) \cdot e^{-j\Delta\phi_{i1}}$ rotates the phase of $y_i(t)$ to align with the signals of the first antenna. After combining the weak signals of multiple antennas, MALoRa will feed the obtained SNR-enhanced signals (i.e., $Y_{combine}(t)$) into a standard LoRa demodulation and decoding pipeline for symbol demodulation and payload data extraction.

We assume that M antennas of a gateway receive the same packet with almost the same signal strength, and the noises at each antenna follow the same compound Gaussian distribution [26]. Ideally, the signal amplitude of a LoRa packet is expected to increase by $M\times$ after coherent combining. In contrast, the amplitude of combined noise increases by $\sqrt[2]{M}\times$. Therefore, the SNR gain of multiple antennas can be represented as below. MALoRa can theoretically achieve 3 dB SNR gain with $M = 2$ antennas and 9 dB gain with $M = 8$ antennas.

$$G_{SNR} = 10 \lg \frac{M^2}{(\sqrt[2]{M})^2} = 10 \lg M \tag{12}$$

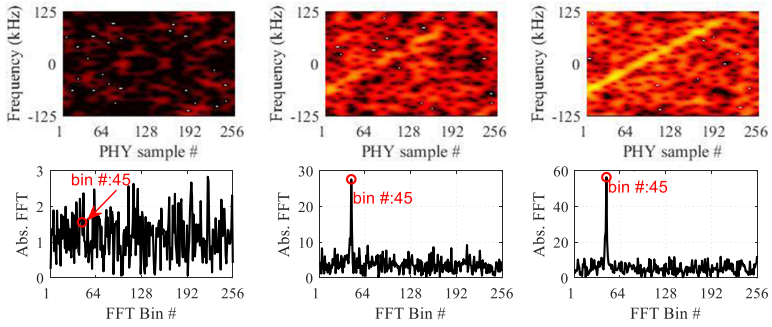

Fig. 9. Coherent combining with different number of antennas (SNR = −30 dB). (a) Standard LoRa demodulation without combining, (b) combine with 4 antennas, and (c) combine with 8 antennas.

Note that different types of noise sources can impact the performance of MALoRa. In real-world scenarios, MALoRa can be affected by both environmental-dependent noises (and interference) and independent noises (i.e., antennas' thermal noises and quantization errors). If we only consider noises from the environment, they may be correlated. However, even though the environment noises are correlated, they cannot achieve coherent combining as LoRa signals. For example, suppose there is a co-existing node in the environment. Since the wireless channels from the co-existing node to multiple antennas are different, their signals cannot coherent combine, if we do not intentionally measure and compensate for their differences. As a result, the sum of noises or interference in the environment will be much lower than LoRa signals. In our manuscript, for simplicity, we assume the noises at each antenna are compound Gaussian noises [26]. The theoretical analysis on noise adding-up results after combining multiple chirps in Section 4.1 can also be applied to signal combining of multiple antennas.

Figure 9 presents the results of coherent combining with different numbers of antennas. Figure 9(a) shows the signals of a weak LoRa symbol before coherent combining and signal strength enhancement. The symbol cannot be demodulated due to ultra-low SNRs. As the weak signals of more antennas are added constructively, we observe the LoRa chirp starts to emerge in the spectrogram shown in Figure 9(b) when we combine the signals received by four antennas, and become clearer when we combine the signals of eight antennas in Figure 9(c). Accordingly, the FFT magnitude of the demodulated frequency becomes higher as more antennas are combined. Finally, the symbol of a weak packet can be correctly demodulated with the combined signals of multiple antennas.

4.3 Handling Instability and Mobility

In the above design, we propose to pull up the SNR of channel phase difference by aggregating other parts of a packet (e.g., sync words, SFD, and payload) in addition to preamble. It is based on an assumption that all LoRa chirps of the same packet pass through the same wireless channel. In practice, however, the channel may vary during the transmission of a LoRa packet due to environment dynamics or node mobility.

To examine the impact of channel dynamics on the measurements of phase difference (i.e., $\Delta\phi_{ij}$) across symbols, we first conduct experiments with high SNR. Figure 10 presents the results of measured channel phase difference across symbols in three different states, namely, (a) static transceiver, (b) static transceiver with persons walking in between, and (c) static transmitter but receiver moves at walking speed. We can observe that in a static state, the measured channel phase

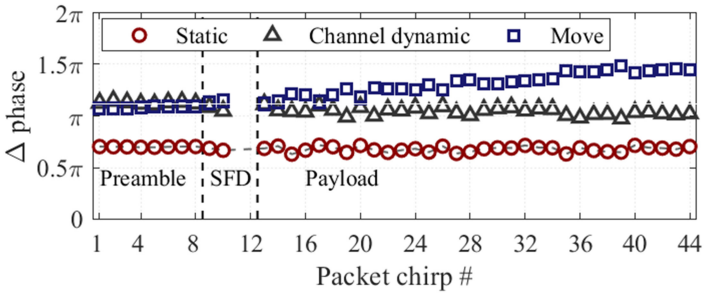

Fig. 10. Measured channel phase difference between h_1 and h_2^* across symbols within a LoRa packet in different states under high SNR (SNR = 20 dB).

differences are almost stable along with time. Results of the dynamic state show similar pattern to the static state. However, the channel phase difference measured by a moving receiver shows obvious changes across different parts of a packet. The phase-changing range of the channel component can be as large as 0.5π. This is reasonable because different moving directions/speeds will change the distance difference between the transmitter and receiver antennas and thus the channel phase difference.

In practice, when the transceiver keeps static, we can combine both preamble and payload to strengthen the signal energy of $h_1 \cdot h_2^*$. Although the channel phase difference may vary a little due to multipath and interference, such variations are limited during a packet transmission and have a negligible effect on coherent combining. In contrast, when the transmitter or the receiver is moving, the channel phase difference changes considerably. In this case, combining preamble and payload may result in a deviation of measured phase difference from the one that can achieve coherent combining, leading to degraded performance of MALoRa.

MALoRa adapts to mobile devices by leveraging a short combining window. We can observe from Figure 10 that the channel phase difference between two antennas keeps almost stable within a short time window (e.g., five chirps). MALoRa uses a short sliding window to obtain stable channel phase difference to ensure constructive combining of multiple antennas. Note that the obtained $\Delta\phi'_{ij}$ for a LoRa symbol may deviate from the ground truth of $\Delta\phi_{ij}$ between two antennas. Using $\Delta\phi'_{ij}$ will not achieve perfect coherent combining. However, this method can still add up symbols constructively and thus can still enhance the SNR of the weak LoRa signals. We validate the effectiveness of this method in low moving speed scenario in Section 6.

In practice, MALoRa may adjust the sliding window length according to the transceiver's moving speed or changing rate of channel phase difference. However, for transceivers with higher moving speed, $\Delta phase$ may change faster, and the time window of a relatively stable $\Delta phase$ will be shorter. In this case, one possible solution is to characterize $\Delta phase$ with a linear model instead of a constant model. This method may help MALoRa to extract $\Delta phase$ with high accuracy and compensate it with fine-grained time granularity. We note that MALoRa aims at relatively static and low speed scenarios and we leave the extension to high speed scenarios as future work.

4.4 Integration with LoRaWAN

MALoRa relies on the accumulated signal energy of multiple preamble chirps to detect weak LoRa packets. Commodity LoRa radios (e.g., Semtech SX1276) support a maximum preamble length of 65,535 chirps. Though a longer preamble is beneficial for detecting more packets with lower SNRs, an excessively long preamble would incur high communication overhead and consume more energy for LoRa nodes. More importantly, a long preamble may not directly translate to higher

gains for packet decoding. Note that each antenna of MALoRa can leverage signals received by itself (i.e., aggregating multiple identical base chirps in preamble) to detect the arrival of a weak packet. However, an individual antenna cannot demodulate payload by aggregating payload chirps with variant initial frequencies. For payload demodulation, a gateway needs to combine payload signals received at multiple antennas to enhance the SNR. Therefore, once a packet is detected, the SNR gain of payload signals would be limited by the number of antennas employed for coherent combining.

Assume that a gateway has M antennas and a packet is received with the same power strength by all antennas. Each antenna uses a packet detection window in length of N chirps. In the packet detection process, the signal strength is expected to increase by $N\times$ if we combine N base chirps in a detection window. Similarly, in the packet decoding process, as MALoRa combines signals of M antennas, we can expect approximately $M\times$ increase in signal strength in comparison with the raw signals of a single antenna.

In particular, if $N < M$, some weak packets may not be reliably detected, losing the chances of being decoded; if $N \gg M$, a LoRa node will then suffer energy waste due to transmitting of an overlong preamble. We basically require $N \approx M$ to ensure that any detected packet would finally get decoded.

Note that a gateway needs to detect periodic frequency peaks to confirm the arrival of a packet. According to the locking process [9] of a standard LoRa decoder, four periodic peaks are needed to verify the presence of a LoRa packet. Suppose MALoRa uses L periodic peaks to indicate the coming of a packet. The detection window needs to slide at least L times with a step of one chirp length. Thus, we can coarsely estimate the length of preamble (N_{pre}) as below.

$$N_{pre} = (L-1) + N \approx (L-1) + M \tag{13}$$

MALoRa employs an adaptive preamble strategy to balance between communication performance and overhead. A LoRa node can coordinate with a gateway to negotiate on the change of preamble length. Specifically, the initial configuration of preamble length is calculated according to Equation (13), which can be performed when the node first joins a LoRaWAN network. The node can adjust preamble length to adapt to new network conditions. In the current implementation, the preamble length of each LoRa node is empirically configured to strike a balance between reception performance and communication overhead. In the future, we plan to optimize the parameter configuration by jointly considering channel dynamics, battery life, and decoding capabilities of gateway.

5 DISCUSSION

Comparison with beamforming. Beamforming [21] is a common technique to strengthen signal reception. It employs multiple antennas and changes the phase shift between antennas to strengthen signals in a specific direction. However, in ultra-low SNR conditions, a beamforming gateway finds it challenging to detect the arrival of a packet since it does not have channel phase information as a priority. Though beamforming systems may search in different directions to detect a LoRa packet, these systems may fail in ultra-low SNR scenarios. Since LoRa has a long symbol duration, a gateway suffers from a long searching time and coarse-grained searching degree, which further degrades the performance. Besides, even if a beamforming gateway finally detects the arrival of a weak packet, it needs to re-search the direction of the next packet because the channel condition changes over time. This requirement also increases the computation overhead at the receiver. In contrast, MALoRa does not need to search, and it calculates the channel phase difference with high accuracy at one shot. The key difference between MALoRa and beamforming is that while beamforming requires active search in all directions and re-search for new incoming

Fig. 11. Implementation.

packets, MALoRa calculates the channel phase difference directly and passively, regardless of where the packet comes from. As such, MALoRa does not incur extra overhead in channel measurements. We evaluate the performance of beamforming in Section 6.

Comparison with MIMO. Multiple input and multiple output (MIMO) antennas are commonly used in many wireless systems, for example, WiFi. A MIMO system uses space diversity or spatial multiplexing generated by multiple antennas at transmitter and receiver to improve the reliability of the system and increase the channel capacity, respectively. MALoRa can be seen as a degenerate case of MIMO system (i.e., single input and multiple output) and does not need typical channel measurements which are extremely challenging in ultra-low SNR scenarios. Though the transmitter of a LoRa node only has one antenna, multiple antennas at a gateway can take advantage of different radio paths to get duplicated signals with phase shifts. MALoRa then coherently combines signals received by multiple antennas to increase the signal-to-noise ratio in harsh environments. We note that MALoRa targets for uplink packets reception from a LoRa node to a gateway. Current commodity LoRa gateways do have multiple antennas, making MALoRa convenient to be applied to commodity devices.

6 EVALUATION

6.1 Methodology

Gateway. We build a LoRa gateway (Figure 11) using synchronized USRP SDRs (N210) based on the gr-lora open-source project [27]. We need to use SDRs to gain access to physical layer since commodity devices do not provide PHY layer samples. The USRPs are synchronized with an external clock source (CDA-2990) and PHY samples are collected and processed using a laptop through a 100 Gigabit Ethernet Switch. In practice, a multi-antenna gateway can be built using low-cost components similar to multi-antenna access points [17, 22]. For example, a Raspberry Pi 4 [28] board can be used for PHY sample collection as well [11]. A Raspberry Pi 4 has a Gigabit Ethernet port, two USB 2 ports, and two USB 3 ports that can be used to deliver physical layer samples. In practice, developers can plug low-cost SDR dongles [29] into USBs of a Raspberry Pi to work as a multi-antenna gateway. We leave implementing MALoRa on low-cost off-the-shelf devices as future work.

LoRa nodes. We use commodity LoRa nodes (Figure 11) as transmitters, composed of Dragino LoRa shields [30] and Semtech SX1276 radios. We use Arduino Uno boards to set key parameters of LoRa nodes. We set the default central frequency, **bandwidth (BW)**, **spreading factor (SF)**, **coding rate (CR)**, and transmission power of LoRa communication as 915 MHz, 250 kHz, 8 , 4/8, and 23 dBm, respectively.

Experiment setup. We evaluate MALoRa in a university and neighborhoods spanning 1.08 km $\times$ 1.2 km. The testbed consists of 40 LoRa nodes and a multi-antenna gateway. We place our

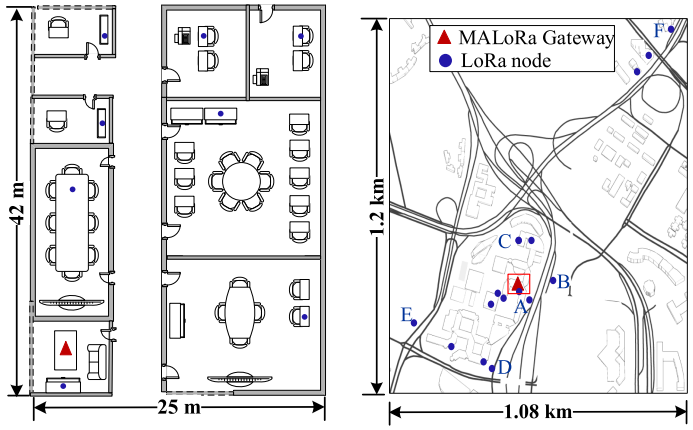

(a) Indoor layout (b) Outdoor layout

Fig. 12. Testbed settings of MALoRa.

Table 2. Preamble Settings

# of chirps in detection window	1	2	4	6	8
# of chirps in preamble	6	6	8	10	12

gateway in one meeting room (Figure 12(a)) inside a building and put LoRa nodes in both indoor and outdoor environments (Figure 12(b)). We configure each node to transmit 50 packets in one measurement and we conduct experiments with a total number of 2,000 measurements.

Metrics. We evaluate the performance of MALoRa with three key metrics: (1) ***Symbol Error Rate (SER)***, (2) ***Packet Reception Ratio (PRR)***, and (3) *Goodput*. We also evaluate the energy consumption of LoRa nodes.

Benchmarks. We conduct comprehensive evaluation and compare the performance against the following benchmarks: (1) *LoRaWAN*—a standard LoRa packet decoder [27]; (2) *Charm* [11]—a distributed LoRa coherent combining scheme; and (3) *Beamforming* — a commonly used technique to strengthen signal reception [21]. We apply beamforming to LoRa by searching the steering phase. Note that the standard LoRa packet decoder (i.e., LoRaWAN) does not use multi-antenna. For fair comparison, we decode signals of each Rx antenna and select the best decoding results as the final results for the standard LoRaWAN.

6.2 Packet Detection Performance

This experiment evaluates the performance of weak packet detection. We set up 10 LoRa nodes and one gateway in an indoor environment. The gateway receives the raw signals of packets transmitted by LoRa nodes. To evaluate the performance of packet detection in a range of different SNRs, we use the gateway to record background noises and add up received noises and packet signals to synthesize signals with various SNR conditions. We then run MALoRa to detect packets from the synthesized low-SNR signals.

Figure 13(a) presents the packet detection results of MALoRa using different packet detection window size when SNR = −35 dB. Packet detection with a single chirp represents the approach used by a standard LoRa receiver. As expected, more than 80 % packets are missed by the standard LoRa packet detection method when SNR is −35 dB. In contrast, the packet detection performance is improved dramatically by MALoRa as it aggregates the power of multiple chirps for packet

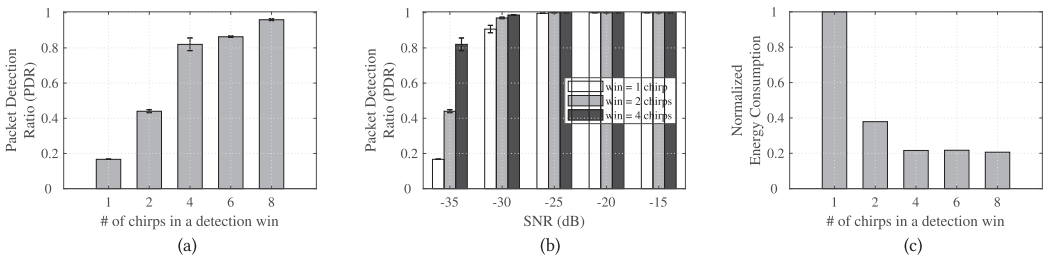

Fig. 13. Packet detection performance of MALoRa: (a) with different length of packet detection window (SNR = −35 dB), (b) under different SNRs, and (c) normalized energy consumption of different length of detection window.

detection. As more chirps are combined in a detection window, the packet detection ratio increases accordingly. For example, more than 82 % packets are detected when we use four chirps in a detection window, meaning that only 18 % of weak packets were missed. The packet detection ratio further increases to 96 % as the length of detection window increases to eight chirps.

Figure 13(b) evaluates packet detection performance under different SNR conditions. We see that the standard LoRa packet detector (i.e., win=1 chirp) can still reliably detect packets when SNR is as low as −25 dB. When SNRs further decreases below −30 dB, however, the packet detection ratio starts to drop dramatically. In contrast, MALoRa still performs well when using four chirps and eight chirps for packet detection. The more chirps combined in a detection window, the more packets can MALoRa detect.

We next evaluate the impact of preamble length and detection window length on the power consumption of LoRa nodes. According to [2], the minimum length of preamble is 6. A receiver needs to detect four periodic peaks to confirm the arrival of a packet. We enlarge the detection window from one chirp to eight chirps and properly configure the length of preamble with the minimum number of required chirps. Settings on the length of preambles and detection windows are shown in Table 2. We assume that a miss detected packet will be re-transmitted and such re-transmission increases the energy consumption of LoRa nodes.

Figure 13(c) reports the average energy consumption of packet detection under different detection window settings. We calculate the energy consumption of a LoRa node based on the datasheet of Semtech SX1276 [2]. The results are normalized to the energy consumption of a standard LoRa node which transmits packets with six chirps in preambles and the gateway uses a one-chirp detection window to detect packets. We observe that the normalized energy consumption of larger detection windows are smaller than 1, meaning that a larger detection window indeed can reduce the power consumption of a LoRa node as compared with the standard demodulation method. Specifically, a detection window of two chirps saves 62% of energy when the SNR is −35 dB. Detection windows with four, six, and eight chirps save almost 80% energy. Although a larger detection window requires a long preamble which may increase the energy cost of preamble transmitting, it would increase the detection rate of packet in low SNRs, reducing the number of re-transmissions. As a result, the overall energy consumption of a LoRa node decreases.

On the other hand, a longer preamble and detection window and will incur extra power consumption and computation overhead for a gateway. However, note that a gateway is usually deployed with tethered power supplies. The energy consumption is no longer a problem for gateways. As for computation overhead, longer preamble only incurs more FFT and multiplication operations, which can be afforded by gateways. Therefore, longer preamble has little effect on the computation overhead of LoRa gateways.

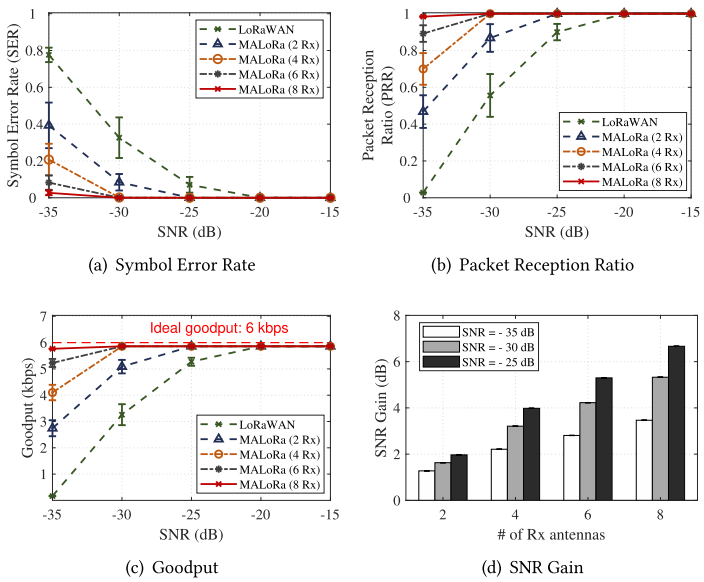

(a) Symbol Error Rate (b) Packet Reception Ratio

(c) Goodput (d) SNR Gain

Fig. 14. Packet decoding performance and SNR gain of MALoRa under different SNRs and different numbers of antennas.

6.3 Packet Decoding Performance

In this subsection, we focus on the packet demodulation performance of MALoRa and evaluate the impacts of various factors. The experiments were conducted both indoors and outdoors. We use 40 LoRa nodes and a gateway with up to eight Rx antennas. In order to evaluate the demodulation performance with low SNRs, we deploy LoRa nodes far away from the gateway and also deeply inside a building, separating the nodes from the gateway by a number of concrete walls. The gateway collects PHY samples when commodity LoRa nodes transmit packets in different locations. We run MALoRa to detect and demodulate packets with different SNR conditions.

Decoding performance. Figure 14 presents the decoding performance of MALoRa in different SNRs. The results of 1 Rx correspond to a standard LoRa decoder without assistance of multiple antennas, which is displayed as a baseline for performance evaluation of MALoRa. We see that the standard LoRaWAN method can correctly demodulate packets when SNRs are as low as −20 dB. As shown in Figure 14(a), the symbol error rates increase as SNRs decrease from −25 dB to −35 dB. In particular, when SNR is −35 dB, 80 % of the symbols are incorrectly demodulated. Such symbol errors cannot be corrected by the error correcting schemes adopted by LoRa standard, resulting in a packet reception ratio of nearly 0 as shown in Figure 14(b).

In contrast to the high symbol error rates of the standard LoRaWAN decoder (i.e., 1 Rx), more symbols can be correctly demodulated by MALoRa even when SNRs drop below −25 dB. Moreover, the symbol error rates of MALoRa can be reduced as we coherently combine more antennas of the gateway. As shown in Figure 14(a) and (b), when MALoRa combines eight Rx antennas, the symbol error rate is retained below 5 % and almost all packets are received since the small number of symbol errors can be corrected by the error correcting codes. In comparison with the standard LoRaWAN decoder, MALoRa (8 Rx) produces an SNR gain of about 10 dB, which can effectively translate to longer communication ranges as well as longer battery life for LoRa nodes in practice.

Figure 14(c) evaluates the goodput of MALoRa under different SNRs. As expected, the goodput of the standard decoder decreases from 6 kbps to nearly 0 kbps as the SNR decreases to −35 dB. The goodputs of MALoRa with two, four, and six antennas exhibit a similar trend. As more antennas

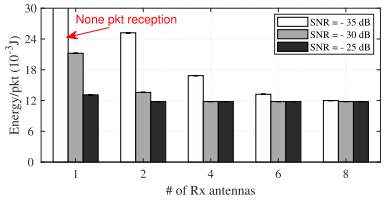

Fig. 15. Energy consumption of MALoRa.

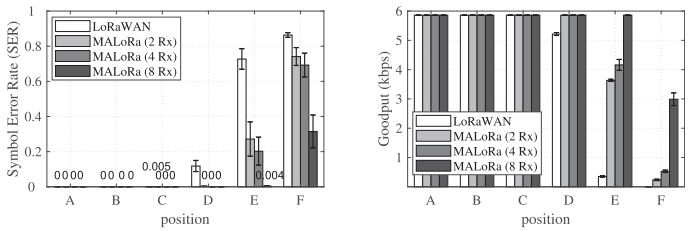

(a) Symbol Error Rate (SER) (b) Goodput

Fig. 16. Effectiveness of MALoRa on extending the communication range: (a) Symbol error rate, and (b) Goodput.

are combined, higher goodputs are produced when SNR < -20 dB. The goodput of MALoRa with eight Rx approaches to the maximum possible goodput in all SNR conditions, since almost all transmitted symbols can be corrected demodulated.

Figure 14(d) evaluates the SNR gain of multiple antennas. We use the SNR before combining as the baseline. We define SNR gain as the SNR improvement produced by multi-antenna combination. We can observe that the SNR gain increases as the number of Rx antennas increases. MALoRa can achieve as high as 6.6 dB SNR gain when the original SNR is -25 dB. We can also observe that MALoRa achieves higher SNR gain when the baseline SNR is higher. Higher SNR gains are achieved when the baseline SNR becomes higher. This is because MALoRa can get more accurate estimation of the channels when the physical channel has higher SNRs, which can result in better combining effects for the signals of multiple antennas.

Energy performance. In the following, we evaluate the energy performance of MALoRa. To this end, we transmit a sequence of identical packets using a LoRa node and record the received PHY samples with multiple antennas of a gateway. We consider a simplified scenario where a packet will be retransmitted if it cannot be decoded correctly. On the other hand, if a packet can be correctly decoded, we consider the next packet as a new packet. We calculate the average energy consumption of transmitting a packet based on the datasheet of Semtech SX1276 [2] and report the energy consumption per packet transmission in Figure 15.

As expected, a node generally consumes less energy to transmit a packet in higher SNRs when the same number of antennas are used for packet decoding. Under the same SNR conditions, the per-packet energy consumption decreases as more antennas are used in coherent combining. Take the case of SNR = -35 dB as an example. The per-packet energy consumption is 25 mJ when MALoRa uses two antennas for packet decoding. The energy consumption decreases to 11 mJ as the number of antennas increases to eight, resulting in 56 % energy savings. When the channel condition is good (e.g., SNR = -25 dB), the marginal gain of using more antennas decreases, since almost all packets can be correctly decoded with fewer antennas already.

Effectiveness on extending the communication range. This experiment evaluates the performance of MALoRa on extending the communication range. We conduct this experiment in an

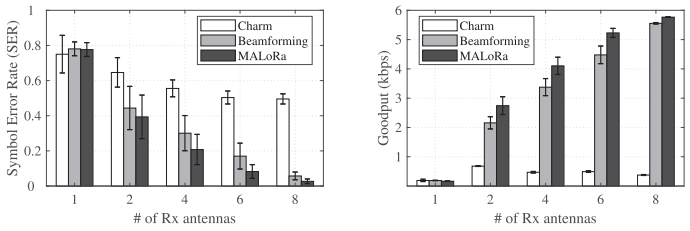

(a) Symbol Error Rate (SER) (b) Goodput

Fig. 17. Performance comparison with state-of-the-art: (a) Symbol error rate, and (b) Goodput.

outdoor environment in an urban city with dense buildings. Figure 12(b) shows the testbed and A to F are six typical positions that are selected to illustrate the communication performance. We set a LoRa node in these positions as a transmitter. F is approximately 960 m away from the gateway, which is the furthest distance we test. To validate the performance of MALoRa, we use a standard LoRa packet decoder and an MALoRa gateway with multiple antennas at the same place to decode LoRa packets. Figure 16(a) and (b) report the SERs and goodput at different distances, respectively.

In Figure 16, we observe that both the standard LoRa decoder and MALoRa can decode packets correctly from A, B, and C, which are within 200 m of the receivers. However, a standard LoRa decoder has an SER of 11.8 % in position D (around 250 m from the transmitter) where MALoRa can still decode all packets with 0 SER. MALoRa extends communication distance by combining more antennas. For example, at position E, standard LoRaWAN fails to communicate with the gateway (72.7 % of SER and 0.352 kbps of goodput). While MALoRa with eight antennas achieves an SER of 0.04 %, much better than standard LoRa as well as MALoRa witha lower number of antennas (27.2 %, 20.3 % for 2 Rx and 4 Rx, respectively). Interestingly, the distance from E to the gateway is almost the same as that from D to the gateway. However, the SER of the standard LoRa decoder in position E is 5× higher than that in position D. This is because the transmitter in position E suffers severe blockage. We note that MALoRa can still achieve almost 0 SER even under severe blockage. Similar cases do exist in real-world IoT applications. For example, a LoRa node may be deployed deep inside a building. As the distance further increases, the performance of MALoRa decreases. However, MALoRa can still achieve more than half of the ideal goodput. In summary, MALoRa can extend the communication range of LoRa to almost 4× of that of a standard LoRa decoder in urban environments.

Comparison against the state-of-the-art. In this experiment, we compare the performance of MALoRa with beamforming and Charm in decoding the same packets when SNR = −35 dB. In Figure 17, we see that the SERs of these three methods remain at the same level when multi-antenna is not used (i.e., 1 Rx). As the number of antennas increases to eight, the SER of MALoRa decreases to 4 %, whereas the SER of Charm and beamforming are still as high as 56 % and 30 % respectively when eight antennas are used. When SNR is low, we find that Charm cannot reliably estimate and calibrate frequency and timing offsets among multiple distributed antennas. Moreover, as the clocks of distributed antennas drift differently, it is extremely difficult to compensate for the frequency drifts during packet transmissions. As a result, the signals received by multiple distributed antennas cannot be aligned and sometimes suffer destructive combining, which substantially affect symbol demodulation performance. Note that the SERs of beamforming decrease gradually as the number of Rx antennas increases. The beamforming method requires searching channel phase difference for every packet; the granularity of phase searching improves as the number of antennas increases, which benefits phase difference measurement and thus results in better alignment of signal combination. However, MALoRa still achieves the best performance as the number of Rx antennas increases.

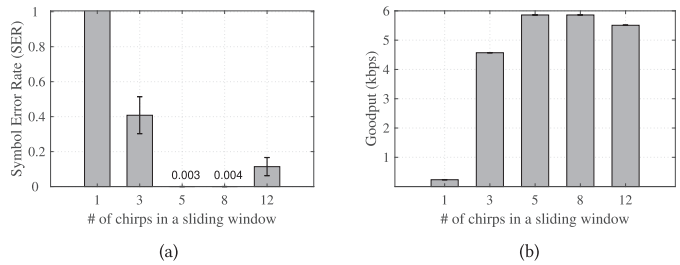

Fig. 18. Impact of mobility (SNR = −35 dB and Rx = 6): (a) Symbol error rate, and (b) Goodput.

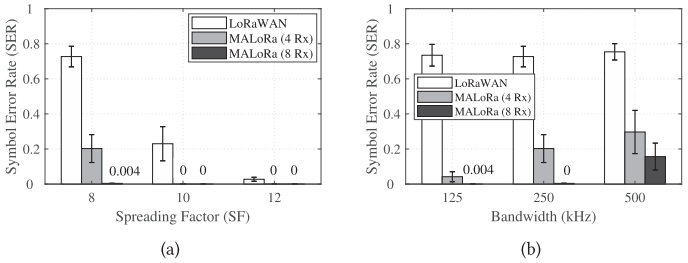

Fig. 19. Impact of LoRa packet configuration (SNR = −35 dB): (a) Spreading factor, and (b) Bandwidth.

Moreover, as a packet with high SERs (e.g., >20 %) cannot be correctly received, the goodput of Charm remains lower than 1 kbps as shown in Figure 17(b). In contrast, the goodput of MALoRa increase almost linearly up to 5.8 kbps as the number of antennas increases from one to eight. Beamforming achieves higher goodput than Charm but lower goodput than MALoRa.

Impact of mobility. As illustrated in Figure 10, if a node moves, the channel phase difference between two antennas may also change across symbols of a packet. In this experiment, we evaluate the impact of node mobility. We conduct this experiment on our campus, and we configure the SNR to −35 dB. A gateway with six receiving antennas is fixed, and a LoRa node is moved at walking speed. Figure 18 show the performance of MALoRa with different lengths of the sliding window.

Figure 18(a) illustrates the performance in terms of SER. We can see that when the length of the sliding window is 1 chirp, the gateway can hardly decode symbols right. The extracted phase differences between antenna pairs are severely affected by noise and interference when the sliding window is too short. Consequently, the combining of signals from six antennas may not result in a constructive addition. As the sliding window becomes longer, the SER of MALoRa decreases, and it achieves 0 when the number of chirps in a sliding window is five or eight. We note that when the number of chirps in a sliding window is 12, the SER increases. The reason is that a longer phase extraction window lowers the accuracy of the phase difference between antennas when the wireless channel changes fast. Therefore, signals from multiple antennas may not be perfectly aligned. Figure 18(b) reports similar results in terms of Goodput. MALoRa achieves the best performance when adopting a sliding window length of 5 or 8 chirps. In real-world applications, we can adjust the length of the sliding window according to the moving speed or changing rate of channel phase difference.

Impact of packet configuration. This experiment examines the impact of LoRa packet configuration on MALoRa performance when SNR = −35 dB.

We first vary **Spreading Factor (SF)** of LoRa packets from eight to 12. Experiment results are shown in Figure19(a). Generally, MALoRa performs better with larger SF. This result is consistent

with the performance of a standard LoRa decoder. We notice that MALoRa with more Rx antennas can achieve more accurate decoding result when SF is small. For example, when SF = 8, the standard LoRa packet decoder (i.e., 1 Rx) has SER of 72 %, while MALoRa with four Rx antennas achieves SER of 20.3 % and MALoRa with eight Rx antennas further improves the decoding accuracy with SER of 0.4 %. This experiment results indicate that a LoRa node can select a small SF to save energy when a gateway is equipped with multiple Rx antennas.

We then vary Bandwidth of LoRa packets. Specifically, we evaluate MALoRa with BW = 125 kHz, 250 kHz, and 500 kHz, respectively. Figure 19(b) represents the results. We observe that MALoRa performs better with smaller bandwidth and more Rx antennas can help decrease the symbol error rate. An interesting observation is that in ultra-low SNR scenarios (SNR = −35 dB), increasing bandwidth will not improve the demodulation performance. This is because the energy of one LoRa chirp is limited and spread across a certain frequency band. As the bandwidth increases, the energy of noise within that frequency band also increases. Therefore, when SNR is extremely low, packets with larger bandwidth become even harder to be decoded correctly.

7 RELATED WORK

Recent years have witnessed substantial advances in LoRa technology such as performance measurement and optimization [31, 32], media assess control [33, 34], concurrent transmissions [3, 35–39], and LoRa backscatter [40].

Latest advances in LoRa communication range enhancement [11, 12, 20, 41] exploit multiple distributed gateways and joint decode at a centralized cloud server. For example, Charm [11] designs a coherent decoder which aggregates raw physical layer samples of multiple distributed gateways and tries to coherently combine them to boost the SNRs of LoRa signals. Chime [12] uses multiple gateways to estimate the optimal operating frequency for signal strength improvement and power consumption reduction. OPR [20] collects the link layer information across multiple gateways to a centralized cloud server and corrects corrupted bits. Although these approaches can achieve better performance than an individual gateway, they typically require sample-level time-synchronization among distributed gateways, which is extremely hard to achieve in practice for commodity LoRa gateways. Besides, various factors influence the performance of coherent combining such as CFOs and STOs across distributed gateways [35]. Moreover, these approaches incur high network traffic since a large volume of raw physical layer samples need to be transmitted to a centralized server. Recent work NELoRa [15] employs mask-enabled deep neural networks to support ultra-low SNR LoRa communication. However, this method involves high computation overhead and needs different models for different parameter configurations.

Our work is related to the single input multiple output technology in information theory [18, 42] in which multiple antennas at the receiver are used to improve packet reception performance. Such works typically require accurate channel measurements to align the signals which is hard to achieve for LoRa especially when wireless channel condition is poor. In this paper, we overcome a series of practical challenges (e.g., packet detection in low SNR, coherent combining without active channel measurement).

Recent works aim to support concurrent transmissions for LoRa [39, 43–47]. Choir [35] aims to support LoRa concurrent transmissions by exploiting the frequency offsets introduced by LoRa hardware. FTrack [3] leverages the time misalignment of LoRa chirps to resolve LoRa collisions. While PCube [47] uses wireless channel phase information to separate collided symbols. NScale [45] amplifies the time offsets between colliding packets with non-stationary signal scaling. Our work is orthogonal to these works in that it improves packet detection and coherently combines weak LoRa packets, which can help these concurrent transmission schemes to better recover packet collisions in low SNR scenarios.

8 CONCLUSION

This paper presents the design and implementation of MALoRa which improves LoRa packet reception performance in low SNR scenarios. MALoRa overcomes a series of practical challenges in achieving coherent combining of multiple antennas of a gateway. In particular, MALoRa proposes a new packet detection method that fully leverages long preambles of LoRa packets so that weak packets can still be detected and thus combined in the following demodulation phase. MALoRa proposes a phase-aligned coherent combining method that ensures constructive combining of LoRa signals received at multiple antennas. MALoRa further proposes an enhanced method to adapt to mobile devices, which expands the application scenarios of LoRa. Our experiment results show that the collocated antennas of a gateway can still provide sufficient spatial diversity that can be harvested to boost weak LoRa packet reception performance.

REFERENCES

[1] LoRa Alliance. 2020. LoRaWAN for developer. In https://lora-alliance.org/lorawan-for-developers.

[2] Semtech. 2020. Semtech SX1276: 137MHz to 1020MHz long range low power transceiver. In https://www.semtech.com/products/wireless-rf/lora-transceivers/sx1276.

[3] Xianjin Xia, Yuanqing Zheng, and Tao Gu. 2020. FTrack: Parallel decoding for LoRa transmissions. *IEEE/ACM Transactions on Networking* 28, 6 (2020), 2573–2586.

[4] Xianjin Xia, Yuanqing Zheng, and T. Gu. 2020. LiteNap: Downclocking LoRa reception. In *IEEE INFOCOM 2020 - IEEE Conference on Computer Communications*. 2321–2330.

[5] Yao Peng, Longfei Shangguan, Yue Hu, Yujie Qian, Xianshang Lin, Xiaojiang Chen, Dingyi Fang, and Kyle Jamieson. 2018. PLoRa: A passive long-range data network from ambient LoRa transmissions. In *Proceedings of the 2018 Conference of the ACM Special Interest Group on Data Communication*. 147–160.

[6] Ningning Hou and Yuanqing Zheng. 2020. CloakLoRa: A covert channel over LoRa phy. In *2020 IEEE 28th International Conference on Network Protocols (ICNP'20)*. IEEE, 1–11.

[7] Lili Chen, Jie Xiong, Xiaojiang Chen, Sunghoon Ivan Lee, Kai Chen, Dianhe Han, Dingyi Fang, Zhanyong Tang, and Zheng Wang. 2019. WideSee: Towards wide-area contactless wireless sensing. In *Proceedings of the 17th Conference on Embedded Networked Sensor Systems*. 258–270.

[8] Yuguang Yao, Zijun Ma, and Zhichao Cao. 2019. LoSee: Long-range shared bike communication system based on LoRaWAN protocol. In *EWSN*. 407–412.

[9] Ningning Hou, Xianjin Xia, and Yuanqing Zheng. 2021. Jamming of LoRa PHY and countermeasure. In *IEEE INFOCOM 2021-IEEE Conference on Computer Communications*. IEEE.

[10] Jansen C. Liando, Amalinda Gamage, Agustinus W. Tengourtius, and Mo Li. 2019. Known and unknown facts of LoRa: Experiences from a large-scale measurement study. *ACM Transactions on Sensor Networks (TOSN)* 15, 2 (2019), 1–35.

[11] Adwait Dongare, Revathy Narayanan, Akshay Gadre, Anh Luong, Artur Balanuta, Swarun Kumar, Bob Iannucci, and Anthony Rowe. 2018. Charm: Exploiting geographical diversity through coherent combining in low-power wide-area networks. In *2018 17th ACM/IEEE International Conference on Information Processing in Sensor Networks (IPSN'18)*. IEEE, 60–71.

[12] Akshay Gadre, Revathy Narayanan, Anh Luong, Anthony Rowe, Bob Iannucci, and Swarun Kumar. 2020. Frequency configuration for low-power wide-area networks in a heartbeat. In *17th USENIX Symposium on Networked Systems Design and Implementation (NSDI'20)*. 339–352.

[13] Yuxiang Lin, Wei Dong, Yi Gao, and Tao Gu. 2020. SateLoc: A virtual fingerprinting approach to outdoor LoRa localization using satellite images. In *2020 19th ACM/IEEE International Conference on Information Processing in Sensor Networks (IPSN'20)*. IEEE, 13–24.

[14] Xianjin Xia and Yuanqing Zheng. 2020. Connecting LoRaWANs deep inside a building. In *Proceedings of the 7th ACM International Conference on Systems for Energy-Efficient Buildings, Cities, and Transportation*. 312–313.

[15] Chenning Li, Hanqing Guo, Shuai Tong, Xiao Zeng, Zhichao Cao, Mi Zhang, Qiben Yan, Li Xiao, Jiliang Wang, and Yunhao Liu. 2021. NELoRa: Towards ultra-low SNR LoRa communication with neural-enhanced demodulation. In *Proceedings of the 19th ACM Conference on Embedded Networked Sensor Systems*. 56–68.

[16] Yaxiong Xie, Yanbo Zhang, Jansen Christian Liando, and Mo Li. 2018. SWAN: Stitched WiFfi antennas. In *Proceedings of the 24th Annual International Conference on Mobile Computing and Networking*. 51–66.

[17] Youwei Zeng, Dan Wu, Jie Xiong, Enze Yi, Ruiyang Gao, and Daqing Zhang. 2019. FarSense: Pushing the range limit of WiFi-based respiration sensing with CSI ratio of two antennas. *Proceedings of the ACM on Interactive, Mobile, Wearable and Ubiquitous Technologies* 3, 3 (2019), 1–26.

[18] Clayton Shepard, Hang Yu, Narendra Anand, Erran Li, Thomas Marzetta, Richard Yang, and Lin Zhong. 2012. Argos: Practical many-antenna base stations. In *Proceedings of the 18th Annual International Conference on Mobile Computing and Networking*. 53–64.
[19] Semtech. 2020. DataSheet Sx1276/77/78/79. In https://www.semtech.com/products/wireless-rf/lora-core/sx1276.
[20] Artur Balanuta, Nuno Pereira, Swarun Kumar, and Anthony Rowe. 2020. A cloud-optimized link layer for low-power wide-area networks. In *Proceedings of the 18th International Conference on Mobile Systems, Applications, and Services (MobiSys'20)*. 247–259.
[21] Fusang Zhang, Zhaoxin Chang, Jie Xiong, Rong Zheng, Junqi Ma, Kai Niu, Beihong Jin, and Daqing Zhang. 2021. Unlocking the beamforming potential of lora for long-range multi-target respiration sensing. *Proceedings of the ACM on Interactive, Mobile, Wearable and Ubiquitous Technologies* 5, 2 (2021), 1–25.
[22] Arliones Hoeller, Richard Demo Souza, Onel L. Alcaraz López, Hirley Alves, Mario de Noronha Neto, and Glauber Brante. 2018. Analysis and performance optimization of LoRa networks with time and antenna diversity. *IEEE Access* 6 (2018), 32820–32829.
[23] Mohamed N. Mahfoudi, Gayatri Sivadoss, Othmane B. Korachi, Thierry Turletti, and Walid Dabbous. 2019. Joint range extension and localization for low-power wide-area network. *Internet Technology Letters* 2, 5 (2019), e120.
[24] LORIOT. https://docs.loriot.io/display/LNS5/Antenna+Configuration.
[25] Yeong-Rok Kim, Jun-Hyun Park, Jae-Mo Kang, Dong-Woo Lim, and Kyu-Min Kang. 2022. Deep learning-aided downlink beamforming design and uplink power allocation for UAV wireless communications with LoRa. *Applied Sciences* 12, 10 (2022), 4826.
[26] David Tse and Pramod Viswanath. 2005. *Fundamentals of Wireless Communication*. Cambridge University Press.
[27] Gr-LoRa GitHub community. 2021. gr-lora Projects. (Jul. 2021). Retrieved Mar. 15, 2021 from https://github.com/rpp0/gr-lora.
[28] Raspberry Pi. Raspberry Pi 4. https://www.raspberrypi.com/products/raspberry-pi-4-model-b/.
[29] RTL-SDR. RTL-SDR. https://www.raspberrypi.com/products/raspberry-pi-4-model-b/.
[30] Dragino. 2021. LoRa Shield for Arduino. (March 2021). Retrieved Mar. 25, 2021 from http://www.dragino.com/products/module/item/102-lora-shield.html.
[31] Li Liu, Yuguang Yao, Zhichao Cao, and Mi Zhang. 2021. DeepLoRa: Learning accurate path loss model for long distance links in LPWAN. In *IEEE INFOCOM 2021-IEEE Conference on Computer Communications*. IEEE.
[32] Xiong Wang, Linghe Kong, Zucheng Wu, Long Cheng, Chenren Xu, and Guihai Chen. 2020. SLoRa: Towards secure LoRa communications with fine-grained physical layer features. In *Proceedings of the 18th Conference on Embedded Networked Sensor Systems*. 258–270.
[33] Amalinda Gamage, Jansen C. Liando, Chaojie Gu, Rui Tan, and Mo Li. 2020. LMAC: Efficient carrier-sense multiple access for LoRa. In *The 26th Annual International Conference on Mobile Computing and Networking (MobiCom'20)*. Article 43, 13 pages.
[34] Zhuqing Xu, Junzhou Luo, Zhimeng Yin, Tian He, and Fang Dong. 2020. S-MAC: Achieving high scalability via adaptive scheduling in LPWAN. In *IEEE INFOCOM'20*. 506–515.
[35] R. Eletreby, D. Zhang, S. Kumar, and O. Yagan. 2017. Empowering low-power wide area networks in urban settings. In *Proceedings of the Conference of the ACM Special Interest Group on Data Communication (SIGCOMM'17)*. 309–321.
[36] Zhenqiang Xu, Pengjin Xie, and Jiliang Wang. 2021. Pyramid: Real-time LoRa collision decoding with peak tracking. In *IEEE INFOCOM 2021-IEEE Conference on Computer Communications*. IEEE.
[37] Zhenqiang Xu, Shuai Tong, Pengjin Xie, and Jiliang Wang. 2020. FlipLoRa: Resolving collisions with up-down quasi-orthogonality. In *2020 17th Annual IEEE International Conference on Sensing, Communication, and Networking (SECON'20)*. IEEE, 1–9.
[38] Shuai Tong, Zhenqiang Xu, and Jiliang Wang. 2020. CoLoRa: Enabling multi-packet reception in LoRa. In *IEEE INFOCOM 2020-IEEE Conference on Computer Communications*. IEEE, 2303–2311.
[39] Zhe Wang, Linghe Kong, Kangjie Xu, Liang He, Kaishun Wu, and Guihai Chen. 2020. Online concurrent transmissions at LoRa gateway. In *IEEE INFOCOM 2020-IEEE Conference on Computer Communications*. IEEE, 2331–2340.
[40] Xiuzhen Guo, Longfei Shangguan, Yuan He, Jia Zhang, Haotian Jiang, Awais Ahmad Siddiqi, and Yunhao Liu. 2020. Aloba: Rethinking ON-OFF keying modulation for ambient LoRa backscatter. In *Proceedings of the 18th Conference on Embedded Networked Sensor Systems (SenSys'20)*. 192–204.
[41] Akshay Gadre, Fan Yi, Anthony Rowe, Bob Iannucci, and Swarun Kumar. 2020. Quick (and dirty) aggregate queries on low-power WANs. In *2020 19th ACM/IEEE International Conference on Information Processing in Sensor Networks (IPSN'20)*. IEEE, 277–288.
[42] Hien Quoc Ngo, Michail Matthaiou, Trung Q. Duong, and Erik G. Larsson. 2013. Uplink performance analysis of multicell MU-SIMO systems with ZF receivers. *IEEE Transactions on Vehicular Technology* 62, 9 (2013), 4471–4483.
[43] Qianyi Huang, Zhiqing Luo, Jin Zhang, Wei Wang, and Qian Zhang. 2020. LoRadar: Enabling concurrent radar sensing and LoRa communication. *IEEE Transactions on Mobile Computing* 01 (Nov. 2020). DOI: http://dx.doi.org/10.1109/TMC.2020.3035797

[44] Marco Zimmerling, Luca Mottola, and Silvia Santini. 2020. Synchronous transmissions in low-power wireless: A survey of communication protocols and network services. *ACM Computing Surveys (CSUR)* 53, 6 (2020), 1–39.
[45] Shuai Tong, Jiliang Wang, and Yunhao Liu. 2020. Combating packet collisions using non-stationary signal scaling in LPWANs. In *Proceedings of the 18th International Conference on Mobile Systems, Applications, and Services (MobiSys'20)*. 234–246.
[46] Xiong Wang, Linghe Kong, Liang He, and Guihai Chen. 2019. mLoRa: A multi-packet reception protocol in LoRa networks. In *2019 IEEE 27th International Conference on Network Protocols (ICNP'19)*. IEEE, 1–11.
[47] Xianjin Xia, Ningning Hou, Yuanqing Zheng, and Tao Gu. 2021. PCube: Scaling LoRa concurrent transmissions with reception diversities. In *Proceedings of the 27th Annual International Conference on Mobile Computing and Networking*. 670–683.

Received 28 April 2022; revised 28 August 2022; accepted 29 August 2022